# The Gaussian line spread functions of single and array-type ionization chambers

**Hui Khee Looe[1,2], Tenzin Sonam Stelljes[1,2], Dietrich Harder[3] and Björn Poppe[1,2]**

[1]Clinic for Radiation Therapy, Pius-Hospital, Oldenburg, Germany
[2]WG Medical Radiation Physics, Carl von Ossietzky University, Oldenburg, Germany
[3]Prof. em., Medical Physics and Biophysics, Georg August University, Göttingen, Germany

## Introduction

The spatial extension of the air volumes of ionization chambers leads to an effect of weighted spatial signal averaging called the "volume effect". Therefore, the beam profiles and the field-size dependent output factors of photon beams should be measured with detectors with sufficient resolution so that the signal perturbation due to the volume effect is negligible, i.e. so that the dose gradient existing within the geometrical dimensions of the detector has negligible effect. However, many high-resolution detectors such as Si diodes, diamond detectors or even films exhibit unfavorable dosimetric properties such as energy and dose rate dependence (Hoban *et al* 1994, Laub *et al* 1999, Fidanzio *et al* 2000, Griessbach *et al* 2005, Djouguela *et al* 2008). The use of film is associated with a complex calibration process. For small field dosimetry, these detectors have to be cross calibrated, under small field conditions, against a calibrated ionization chamber whose reading may need to be corrected for the volume effect.

These considerations have caused the necessity to quantify the spatial resolution of extended detectors such as ionization chambers, and to devise methods for the correction of their volume effect. In our previous work (Stelljes *et al* 2011), the *line spread functions* or *convolution kernels* of seven common cylindrical ionization chambers have been shown to be closely described by Gaussian distributions. This was accomplished by approximating the ionization chamber's *measured signal profile* $M(x)$ by the convolution product of the *true dose profile* $D(x)$ (measured by a high-resolution Si diode) and a Gaussian kernel $K(x)$ with adaptable standard deviation $\sigma$. For all investigated chambers, the measured $\sigma$ values for both the lateral and longitudinal line spread functions, $\sigma_{lat}$ and $\sigma_{long}$, have been tabulated.

In this work, this table of $\sigma$ values is extended to comprise nine cylindrical ionization chambers, two flat chambers and the single chambers of two 2D ionization chamber arrays. The spatial resolution of the Si diode, with its 1 mm wide sensitive element, is now accounted for by adding in quadrature the $\sigma$ values of the examined ionization chambers, obtained in a first approximation by comparison with the Si diode, and the measured value $\sigma_{Diode}$.

## Materials and methods

The line spread function of the Si diode (type 60012, PTW-Freiburg) was evaluated by comparing the true dose profile of a 6 MV slit beam (FWHM = 2.5 mm) at SSD 73 cm and 15 mm depth in water, measured with EBT3 radiochromic film, with the signal profile of the Si diode detector. The EBT3 measurement films were scanned together with the calibration films using an EPSON 10000XXL scanner in transmission mode at a resolution of 200 dpi. The pixel values in the red and blue channels were extracted from the scanned images; the former were used for the dose evaluation and the latter to correct for the difference in coating thickness. For the calibration films, the mean pixel value of a set of 30 pixels x 30 pixels was used, and the calibration curve was then fitted by a fifth degree polynomial. The dose profile measured with the film was averaged over 5 pixels on both sides of the central axis to reduce the statistical noise. Using the method described above, as shown in Figure 1, the EBT3 dose profile (thin line) was convolved with a Gaussian function whose standard deviation was varied systematically until the best fit with the measured signal profile of the diode was achieved (open circles). The optimal $\sigma_{\text{Diode}}$ value was found to be 0.30 mm. The width of each pixel of the scanned images was 0.127 mm (at a resolution of 200 dpi). By assuming also a Gaussian response function for each pixel with FWHM equal to the pixel size, the $\sigma$ value of the film and scanner combination would be 0.054 mm. When added in quadrature to the 0.30 mm obtained with the diode, the value of the $\sigma_{\text{Diode}}$ is only increased by 0.005 mm, which falls

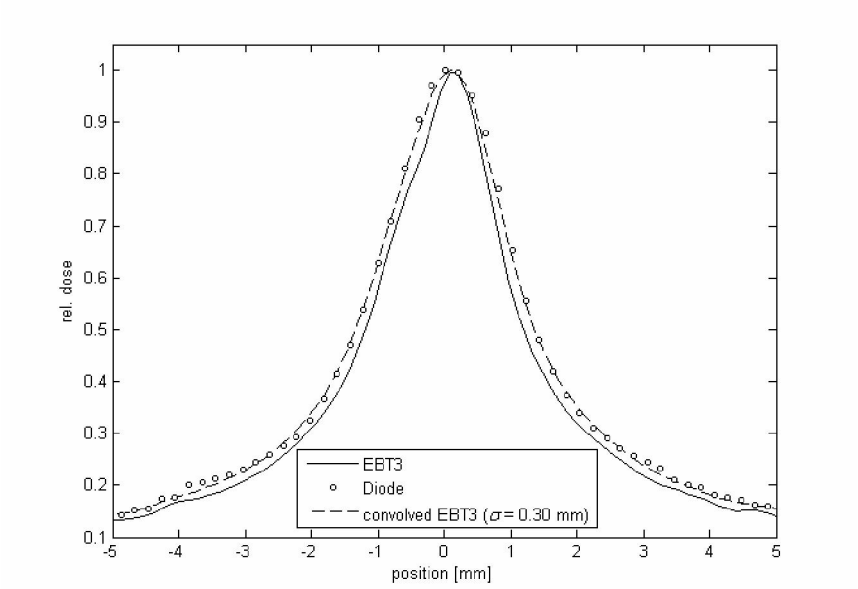


Figure 1: Determination of the line spread function of the Si diode detector at SSD 73 cm and 15 mm depth in water using a 6 MV photon beam. Shown are the measured EBT3 dose profile (thin line), the signal profile measured with the diode (open circles) and the EBT3 dose profile convolved with a Gaussian line spread function having a $\sigma$ = 0.30 mm (dashed line), which $\sigma$ value yields the optimal fit with the Si diode measurement.

within the limit of uncertainty of our measurements. Therefore, the $\sigma_{Diode}$ was determined to be (0.30 ± 0.02) mm. In all following determinations of the line spread functions of ionization chambers, the resolution of the diode was accounted for by adding in quadrature the $\sigma$ values of the examined ionization chambers, obtained in a first approximation by comparison with the diode, and the value $\sigma_{Diode}$ of the diode.

The determinations of the parameters $\sigma_{lat}$ and $\sigma_{long}$ for two PinPoint ionization chambers (Type 31015 and 31016, PTW-Freiburg) were carried out using the same procedure of comparing their measured signal profiles with the Si diode signal profile which was described previously (Stelljes *et al* 2011). For the two flat chambers (Roos chamber type 34001 and Markus chamber type 23343, both from PTW-Freiburg) and the single chambers of the two 2D ionization chamber arrays (729 2D-ARRAY type 10024 and STARCHECK type 10032, both from PTW-Freiburg), the signal profiles were acquired by scanning the chambers across a 4 cm wide beam. All measurements were carried out at 5 cm depth in water, i.e. at depths beyond the depth-dose maximum.

**Results**

Figures 2 and 3, holding for the Roos chamber and the single chamber of the 729 2D-ARRAY at 6 and 15 MV, show that the convolution product of the Si diode signal profile (thick line) with a Gaussian kernel, whose $\sigma$ value is indicated in the figure, agrees very well with the signal profile of the ionization chamber (open circles). Therefore the line spread functions of these chambers can as well be described by Gaussian functions.

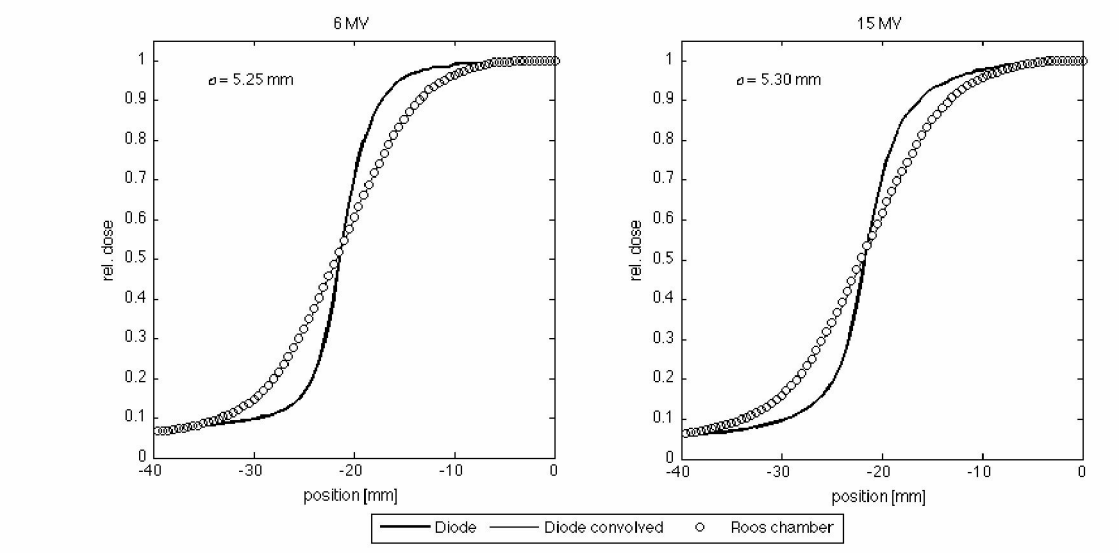


Figure 2: Determination of the line spread function of the Roos chamber (PTW 34001). Beam profiles were obtained by scanning a 4 × 40 $cm^2$ field at (a) 6 MV and 5 cm depth; (b) 15 MV and 5 cm depth.

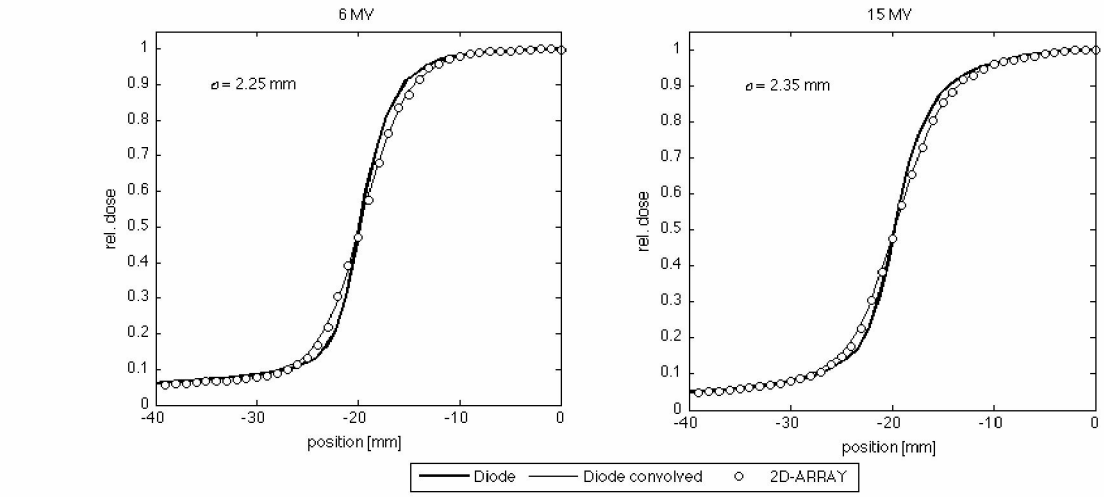


Figure 3: Determination of the line spread function of a single ionization chamber of the 2D array 729 (PTW 10024). Beam profiles were obtained by scanning a 4 × 40 $cm^2$ field at (a) 6 MV and 5 cm depth; (b) 15 MV and 5 cm depth.

The resulting $\sigma$ values of all investigated ionization chambers, corrected with $\sigma_{diode}$ = 0.30 mm by addition in quadrature, have been entered in Table 1.

Table 1. The dimensions of the ionization chambers investigated in this work and the associated standard deviations of their lateral ($\sigma_{lat}$) and longitudinal ($\sigma_{long}$) line spread functions.

| # | Detector | Sensitive volume [$cm^3$] | Diameter of sensitive volume [mm] | Length of sensitive volume [mm] | $\sigma_{lat}$ [mm] 6/15 MV (± 0.02 mm) | $\sigma_{long}$ [mm] 6/15 MV (± 0.02 mm) |
|---|---|---|---|---|---|---|
| 1 | PTW 31014 PinPoint | 0.015 | 2.0 | 5.0 | 0.99/0.99 | 1.98/2.02 |
| 2 | PTW 31015 PinPoint | 0.03 | 2.9 | 5.0 | 1.40/1.49 | 2.23/2.30 |
| 3 | PTW 31016 PinPoint 3D | 0.016 | 2.9 | 2.9 | 1.38/1.38 | 1.78/1.90 |
| 4 | PTW 31010 SemiFlex | 0.125 | 5.5 | 6.5 | 2.20/2.30 | 2.28/2.50 |
| 5 | PTW 31013 SemiFlex | 0.3 | 5.5 | 16.25 | 2.41/2.44 | 4.87/5.05 |
| 6 | IBA CC01 | 0.01 | 2.0 | 3.6 | 0.69/0.71 | 1.18/1.24 |
| 7 | IBA CC04 | 0.08 | 4.0 | 3.6 | 1.49/1.51 | 1.49/1.51 |
| 8 | IBA CC08 | 0.08 | 6.0 | 4.0 | 2.04/2.22 | 1.73/2.00 |
| 9 | IBA CC13 | 0.13 | 6.0 | 5.8 | 2.26/2.38 | 2.26/2.38 |
| 10 | PTW 23343 Markus | 0.055 | 5.3 [a] | - | 2.37/2.45 | - |
| 11 | PTW 34001 Roos | 0.35 | 15.0 [a] | - | 5.26/5.31 | - |
| 12 | PTW 10024 729 2D-ARRAY | 0.125 | 5.0 [b] | 5.0 [c] | 2.27/2.37 | 2.27/2.37 |
| 13 | PTW 10032 STARCHECK | 0.05 | 2.0 [b] | 5.0 [c] | 1.63/1.73 | - |

[a] parallel plate chamber; [b] width of a single array chamber; [c] length of a single array chamber

**Discussion**

In summary, our experiments have shown that the lateral and the longitudinal line spread functions of all investigated *cylindrical ionization chambers, flat chambers and single chambers of 2D ionization chamber arrays* can be characterized by Gaussian functions. This finding is in line with the results of Garcia-Vicente *et al* 1998, Bednarz *et al* 2002, Ulmer and Kaissl 2003, Pappas *et al* 2006, Yan *et al* 2008 and Fox *et al* 2010, who also concluded that the best fitting function to describe the detectors' convolution kernels is the Gaussian distribution. Yan *et al* 2008 used a similar approach to obtain the $\sigma$ values for the IBA CC13 chamber by minimizing the differences between ionization chambers' measured signal profiles and the convolution of the diode measured profiles with Gaussian kernels at different field sizes and depths. They obtained the $\sigma_{lat}$ values 2.71 and 2.79 mm, and no significant depth or field size dependence of $\sigma_{lat}$ was detected. Fox *et al* 2010 investigated the $\sigma_{lat}$ and $\sigma_{long}$ values for the IBA CC01, CC04 and CC13 chambers using analytical fits to both $D(x)$ and $M(x)$. They scanned the dose profiles of a 10 x 10 $cm^2$ field in both the cross-plane and in-plane directions at 6 MV. The average $\sigma_{lat}$ and $\sigma_{long}$ values for the CC01, CC04 and CC13 chambers were 1.52, 1.78 and 2.57 mm and 1.72, 1.99 and 2.64 mm respectively. Their $\sigma$ values were significantly higher than the corresponding values obtained in this work (Table 1). This is probably due to the facts (1) that we used a lengthy field in order to measure the 1D line spread function of a detector under exclusion of any effects of its line spread function at right angles to the direction of the examination, and (2) that we avoided to fit analytical functions such as the error function to the measured $D(x)$ and $M(x)$ profiles, knowing that the convolution kernel determining $D(x)$ is closer to a Lorentz function than to a Gaussian function (Djouguela 2009), (3) that $\sigma$ was "setup dependent" as reported by Fox *et al* 2010, in contrast to the depth independence observed in the present study.

The astounding fact that the line spread function of an ionization chamber has non-zero valued "tails" *reaching beyond the chambers' geometrical boundaries* can be explained as an effect of secondary electron transport. The relationship between the true dose profile $D(x)$ and ionization chamber measured signal profile $M(x)$ is an *indirect* one, mediated by the common photon fluence profile $\Phi(x)$, as depicted in Figure 4. The Gaussian line spread function $K(x)$ results from the combined effect of convolution kernel $K_D(x)$, which relates $\Phi(x)$ and $D(x)$, and kernel $K_M(x)$, which relates $\Phi(x)$ and $M(x)$, as shown in eq. (1) by application of Fourier's convolution theorem:

**Fehler! Textmarke nicht definiert.Fehler! Textmarke nicht definiert.Fehler! Textmarke nicht definiert.Fehler! Textmarke nicht definiert.Fehler! Textmarke nicht definiert.**

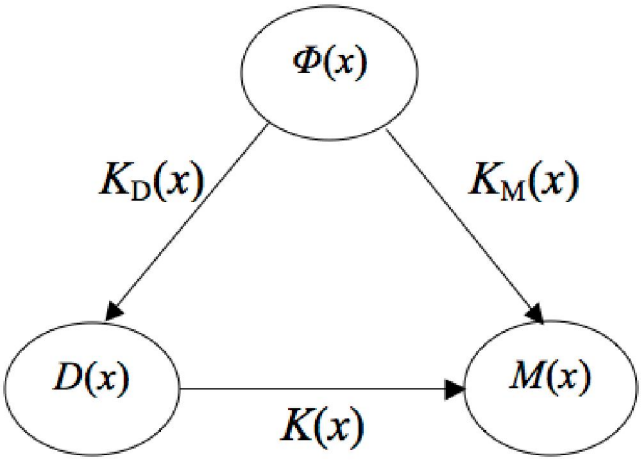


Figure 4: Diagram illustrating the relationship between the photon fluence profile $\Phi(x)$, the true dose profile $D(x)$, the measured signal profile $M(x)$ and the associated convolution kernels.

$$\mathrm{FT}\left[K(x)\right] = \frac{1}{\sqrt{2\pi}}\left[\frac{\mathrm{FT}\left[K_{\mathrm{M}}(x)\right]}{\mathrm{FT}\left[K_{\mathrm{D}}(x)\right]}\right] \qquad (1)$$

Eq. (1) is useful to understand the ubiquity of the Gaussian shape of $K(x)$. The convolution kernel $K_{\mathrm{D}}(x)$ can best be described by a Lorentz function (Djouguela *et al* 2009), but also roughly by a Gaussian. Also $K_{\mathrm{M}}(x)$ may also roughly be considered as a Gaussian. Since the Fourier transforms of Gaussian functions are also Gaussians, and since the quotient of two Gaussians is again a Gaussian, eq. (1) approximately indicates that Gaussian shapes of $K(x)$ have generally to be expected.

The other phenomenon clearly confirmed by our experiments is that Gaussian shapes of $K(x)$ are obtained if the convolution kernels are measured at depths beyond the depth dose maximum, whereas non-Gaussian kernels have been observed *for the same detectors* at shallow depths (Poppe et al 2006, Heidorn et al 2008). This can be explained by the different lateral and angular distributions of the secondary electrons in the dose-buildup region and in the depth region of transient secondary electron equilibrium.

## Conclusion

The present study shows that, at depths beyond the depth-dose maximum, the line spread functions of flat ionization chambers and of the single chambers of 2D ionization chamber arrays can be described by Gaussian distributions, in the same way as those of

cylindrical ionization chambers shown previously. The results from the previous study (Stelljes *et al* 2011) have been supplemented by the $\sigma$ values of two additional PinPoint chambers, the Roos and Markus flat chambers, and the single chambers of the 729 2D-ARRAY and the STARCHECK array. Furthermore, the $\sigma$ values of the ionization chambers examined in this work have been corrected for the limited spatial resolution of the Si diode that was used to approximate the true dose profiles. The line spread function of the Si diode has been determined using an auxiliary experiment in which the Si diode signal profile was compared with a true dose profile measured with EBT3 radiochromic film scanned at high spatial resolution in order to achieve an almost vanishing averaging effect. The phenomenon that the lateral tails of the Gaussian line spread functions are extending beyond the geometrical dimensions of the chambers can be explained by the ranges of the secondary electrons, and the ubiquity of the Gaussian shape of the line spread functions can be approximately understood by considering the underlying complex of convolutions.

## References


Bednarz G, Huq M S and Rosenow U F 2002 Deconvolution of detector size effect for output factor measurement for narrow Gamma Knife radiosurgery beams *Phys. Med. Biol.* **47** 3643-9

Djouguela A, Griessbach I, Harder D, Kollhoff R, Chofor N, Rühmann A, Willborn K and Poppe B 2008 Dosimetric characteristics of an unshielded p-type Si diode: linearity, photon energy dependence and spatial resolution *Z. Med. Phys.* **18** 301-6

Djouguela A, Harder D, Kollhoff R, Foschepoth S, Kunth W, Rühmann A, Willborn K and Poppe B 2009 Fourier deconvolution reveals the role of the Lorentz function as the convolution kernel of narrow photon beams *Phys. Med. Biol.* **54** 2807-27

Fidanzio A, Azario L, Miceli R, Russo A and Piermattei A 2000 PTW-diamond detector: dose rate and particle type dependence *Med. Phys.* **27** 2589-93

Fox C, Simon T, Simon B, Dempsey J F, Kahler D, Palta JR, Liu C and Yan G 2010 Assessment of the setup dependence of detector response functions for mega-voltage linear accelerators *Med. Phys.* **37** 477-84

García-Vicente F, Delgado J M and Peraza C 1998 Experimental determination of the convolution kernel for the study of the spatial response of a detector *Med. Phys.* **25** 202-7

Griessbach I, Lapp M, Bohsung J, Gademann G and Harder D 2005 Dosimetric characteristics of a new unshielded silicon diode and its application in clinical photon and electron beams *Med. Phys.* **32** 3750-4

Heidorn S, Kollhoff R, Willborn K C, Harder D and Poppe B 2008 Über das laterale Ansprechvermögen der Einzelkammern verschiedener Detektor-Arrays 39. *Medizinische Physik 2008 Tagungsband der Jahrestagung Oldenburg (Hrsg. B. Kollmeier)*

Hoban P W, Heydarian M, Beckham W A and Beddoe A H 1994 Dose rate dependence of a PTW diamond detector in the dosimetry of a 6 MV photon beam *Phys. Med. Biol.* **39** 1219-29

Laub W U, Kaulich T W and Nüsslin F 1999 A diamond detector in the dosimetry of high-energy electron and photon beams *Phys. Med. Biol.* **44** 2183-92

Pappas E, Maris T G, Papadakis A, Zacharopoulou F, Damilakis J, Papanikolaou N and Gourtsoyiannis N 2006 Experimental determination of the effect of detector size on profile measurements in narrow photon beams *Med. Phys.* **33** 3700-10

Poppe B, Blechschmidt A, Djouguela A, Kollhoff R, Rubach A and Harder D 2006. Two-dimensional ionisation chamber arrays for IMRT dose verification. Med. Phys. **33** 1005-15

Stelljes T S, Looe. H K, Harder D and Poppe B 2011 Beschreibung der Halbschattenverbreiterung durch das endliche Volumen von Ionisationskammern mit Hilfe von Gaußschen Faltungskernen *Drei-Länder-Tagung Medizinische Physik, ÖGMP-DGMP-SGSMP, ISBN: 3-925218-89-0, Wien*

Ulmer W and Kaissl W 2003 The inverse problem of a Gaussian convolution and its application to the finite size of the measurement chambers/detectors in photon and proton dosimetry *Phys. Med. Biol.* **48** 707-27

Yan G, Fox C, Liu C and Li J G 2008 The extraction of true profiles for TPS commissioning and its impact on IMRT patient-specific QA *Med. Phys.* **36** 3661-70